Chapter 3

Theory of EIT in an Ideal Three-Level System

3.1 Three-Level Systems

So far the interaction of a two-level system (or series of two-level systems) with a near resonant, monochromatic field has been considered. This leads to the Doppler-broadened spectra and saturation spectra as shown in chapter 2 . The three-level system interacting with two monochromatic fields offers a vast array of new physics to be investigated. It is the development of monochromatic tuneable laser sources that has allowed such investigations to be undertaken.

There are essentially three different types of three-level system: Λ; cascade and V. These are shown in Fig. 3.1.

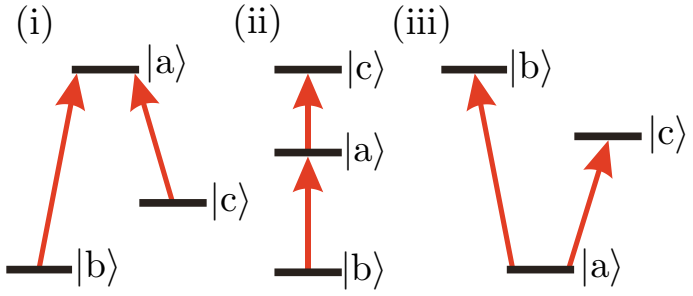

Figure 3.1: The three different three-level systems, with the optical transitions shown by the red arrows. (i) A Λ system, (ii) a cascade system and (iii) a V system.

3.2 Coherent Population Trapping

The application of two continuous-wave (cw) fields to a three-level atomic system puts the atom into a coherent superposition of states. This superposition of states is stable against absorption from the radiation field. Hence this phenomena is referred to as coherent population trapping (CPT).

The Hamiltonian for a three-level system, as shown in Fig. 3.1, is given by,

$$\mathscr{H} = \mathscr{H}_0 + V_1 + V_2 \ . \tag{3.1}$$

$\mathscr{H}_0$ is the bare atom Hamiltonian; V_1 is the potential due to the field with Rabi frequency Ω_1 and angular frequency ω_1; and V_2 is the potential due to the field with Rabi frequency Ω_2 and angular frequency ω_2. The Rabi frequencies are assumed to be real. Here,

$$\mathscr{H}_0 = \hbar\omega_{\rm a}|{\rm a}\rangle\langle{\rm a}| + \hbar\omega_{\rm b}|{\rm b}\rangle\langle{\rm b}| + \hbar\omega_{\rm c}|{\rm c}\rangle\langle{\rm c}| \ , \tag{3.2}$$

$$V_1 = \frac{\hbar}{2}\Omega_1 {\rm e}^{-{\rm i}\omega_1 t}|{\rm b}\rangle\langle{\rm a}| + \frac{\hbar}{2}\Omega_1 {\rm e}^{+{\rm i}\omega_1 t}|{\rm a}\rangle\langle{\rm b}| \ , \tag{3.3}$$

$$\text{and} \quad V_2 = \frac{\hbar}{2}\Omega_2 {\rm e}^{-{\rm i}\omega_2 t}|{\rm c}\rangle\langle{\rm a}| + \frac{\hbar}{2}\Omega_2 {\rm e}^{+{\rm i}\omega_2 t}|{\rm a}\rangle\langle{\rm c}| \ . \tag{3.4}$$

Considering the interaction of this Hamiltonian with the three-level system provides a simple one-atom model of CPT.

It is apparent that the eigenstates of $\mathscr{H}_0$ ($|{\rm a}\rangle$, $|{\rm b}\rangle$ and $|{\rm c}\rangle$) are not eigenstates of $\mathscr{H}$. Instead the eigenstates of $\mathscr{H}$ are linear combinations of $|{\rm a}\rangle$, $|{\rm b}\rangle$ and $|{\rm c}\rangle$. In the case that the two fields are on resonance, ($\omega_1 = \omega_{\rm a} - \omega_{\rm b}$ and $\omega_2 = \omega_{\rm a} - \omega_{\rm c}$), the three eigenstates of $\mathscr{H}$ are,

$$|{\rm C}_1\rangle = \frac{1}{\sqrt{2}}\left(-|{\rm a}\rangle + \frac{\Omega_1}{\sqrt{\Omega_1^2+\Omega_2^2}}|{\rm b}\rangle + \frac{\Omega_2}{\sqrt{\Omega_1^2+\Omega_2^2}}|{\rm c}\rangle\right) \ , \tag{3.5}$$

$$|{\rm C}_2\rangle = \frac{1}{\sqrt{2}}\left(|{\rm a}\rangle + \frac{\Omega_1}{\sqrt{\Omega_1^2+\Omega_2^2}}|{\rm b}\rangle + \frac{\Omega_2}{\sqrt{\Omega_1^2+\Omega_2^2}}|{\rm c}\rangle\right) \ , \tag{3.6}$$

$$|{\rm NC}\rangle = \frac{\Omega_2}{\sqrt{\Omega_1^2+\Omega_2^2}}|{\rm b}\rangle - \frac{\Omega_1}{\sqrt{\Omega_1^2+\Omega_2^2}}|{\rm c}\rangle \ . \tag{3.7}$$

$|{\rm NC}\rangle$ contains no component of $|{\rm a}\rangle$ and hence there is no coupling between these two states. Thus any population in $|{\rm NC}\rangle$ is trapped in that state. Both $|{\rm C}_1\rangle$ and $|{\rm C}_2\rangle$ contain components of $|{\rm a}\rangle$ and hence couple to it.

Over a period of time, dependent upon the rate of spontaneous emission from the excited state, all of the population of the system will build up in $|\mathrm{NC}\rangle$. Hence all of the population becomes coherently trapped in a dark state.

The first experimental realization of CPT was made by Alzetta *et al.*, [45]. In this work the fluorescence of Na atoms was observed. An inhomogeneous magnetic field was applied along the axis of the Na cell. At certain points along the length of the cell the fluorescence disappeared. These "black lines" were due to CPT taking place, in Λ systems, at positions where the magnetic field was such that the CPT resonance was met. A theoretical analysis of the coherence phenomena that lead to these effects was presented by Arimondo and Orriols, [46]. At the same time and independently Whitley and Stroud Jr., [47], produced a theoretical treatment of CPT in a three-level cascade system.

3.2.1 Applications of CPT

CPT has many potential areas of application. Ground states are generally much longer lived than excited states. Measuring the line width of a ground state would potentially increase the resolution of any device, which relied on the width of a spectral feature, by several orders of magnitude. Considering the interactions of two fields with three atomic levels, it is possible to measure a transition with line width orders of magnitude less than the excited state line width. The increase in interest in CPT was largely fuelled by applications in metrology, [48]. More recently there has been significant interest in the field of atomic clocks, [49, 50, 51], where the use of CPT has allowed all optical miniaturised atomic clocks to be produced.

Velocity selective coherent population trapping (VSCPT) is another application of CPT. The technique developed by Aspect *et al.*, [52], requires the formation of a Λ system comprising two degenerate Zeeman ground states with counter-propagating perpendicularly polarized beams. This results in only zero velocity atoms being resonant with the two beams, and thus only zero velocity atoms become trapped in the dark state. Atoms that are not in the correct velocity range for coherent population trapping to take place rely on momentum redistribution, due to optical pumping followed by spontaneous emission, to fall into the correct velocity range for the dark state. This cooling mechanism provides

for laser cooling to below both the Doppler limit and the single-photon recoil energy.

A number of review articles have been written on the subject, including the comprehensive review by Arimondo, [53], and the more recent article by Wynands and Nagel, [20].

3.3 Electromagnetically Induced Transparency

Electromagnetically induced transparency (EIT), [54, 55], is the cancellation of the absorption of a weak probe field. The cancellation is due to the application of a pump field, resonant with one of the levels of the original transition and a third level.

The immediate similarity to CPT is apparent. The difference between EIT and CPT being that CPT tends to refer to two fields of approximately equal Rabi frequency. EIT refers to the regime where one of the fields (pump) is much stronger than the other (probe). In the case of EIT the interest is in how the pump modifies the medium experienced by the probe.

As the only difference between EIT and CPT is the strength of the beams, then the brief theoretical treatment of a three-level system presented above can be extended to the case where, $\Omega_1 \ll \Omega_2$.

It follows from equations 3.5 , 3.6 and 3.7 that the coupling and non-coupling states become,

$$
\begin{aligned}
|\mathrm{C}\rangle &= \frac{1}{\sqrt{2}}|\mathrm{C}_1\rangle + \frac{1}{\sqrt{2}}|\mathrm{C}_2\rangle \ , && (3.8)\\
&= \frac{\Omega_2}{\sqrt{\Omega_1^2+\Omega_2^2}}|\mathrm{c}\rangle \ , && (3.9)\\
&\simeq |\mathrm{c}\rangle \ , && (3.10)\\
|\mathrm{NC}\rangle &= \frac{\Omega_2}{\sqrt{\Omega_1^2+\Omega_2^2}}|\mathrm{b}\rangle \ , && (3.11)\\
&\simeq |\mathrm{b}\rangle \ . && (3.12)
\end{aligned}
$$

Throughout this work the three-level systems under investigation are exclusively Λ-systems. The Λ-system with pump and probe fields is shown in Fig. 3.2.

The induced transparency is caused by the interference of coherences in the

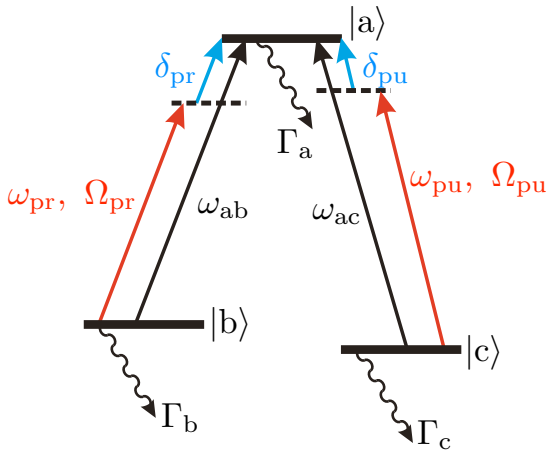

Figure 3.2: A three-level Λ-system. The three levels are linked by two fields, probe and pump. The two fields have angular frequency ω_{pr} and ω_{pu} and Rabi-frequency Ω_{pr} and Ω_{pu}, respectively. The probe field has a detuning from resonance of δ_{pr}, and the pump field a detuning δ_{pu}. Each of the levels $|i\rangle$ has a line width (FWHM) Γ_i.

atomic system. Alongside the modification of the absorption is the concomitant modification of the dispersion, [1, 56], encapsulated in the Kramers-Kronig relations, § 2.3.2. This is what makes EIT of such interest, the steep dispersion is coincident with a transparent window in the medium; normally such steep dispersion would be coincident with significant absorption.

Harris *et al.*, [54], demonstrated theoretically the possibility of rendering a medium transparent on a given allowed transition from a ground state to an excited state. This required the application of a pump beam resonant with a third state and the excited state. The first experimental realization of EIT was by Boller *et al.*, [55]. EIT was observed on a Λ system in strontium vapour. The transmission of a probe was increased from e^{-20} to e^{-1}.

Xiao *et al.*, [57], measured the dispersion due to EIT directly. This was accomplished using a Mach-Zehnder interferometer. The measurements were carried out, on a cascade system, in Rb vapour with the probe resonant with the D_2 transition and the pump resonant with $5P_{3/2} \rightarrow 5D_{5/2}$ transition.

The narrowest recorded EIT resonances in atomic vapours are of ~ 30 Hz in a medium where the excited state line width is 6 MHz, [58]. This means that the transparent window is a factor of 2×10^5 narrower than the Doppler-free

transition in the absence of the pump beam.

In recent years there has been a vast amount of work done in the field of EIT. Some of the more important advances and potential applications are presented in § 1.1.1 . There are a number of good review articles covering this rapidly growing field, [11, 59, 60].

3.4 EIT via Optical-Bloch Equations

Consider an idealized three-level Λ-system as in Fig. 3.2 on the preceding page. There are obvious similarities to the idealized two-level system of Fig. 2.1 on page 12. In the same way that the complex susceptibility, and hence absorption and dispersion, of the two-level medium was calculated in chapter 2, it is possible to calculate the complex susceptibility of the three-level Λ-system. The Hamiltonian for this system is given by equation C.1,

$$\mathscr{H} \;=\; \mathscr{H}_{\rm A} + V_{\rm pr} + V_{\rm pu} \;;$$

The interactions of the atoms with the probe and pump laser fields are given by equations C.8 and C.9 ,

$$\begin{aligned} V_{\rm pr} &= \frac{\hbar\Omega_{\rm pr}}{2}\left(|{\rm a}\rangle\langle{\rm b}|{\rm e}^{{\rm i}\omega_{\rm pr}t} + |{\rm b}\rangle\langle{\rm a}|{\rm e}^{-{\rm i}\omega_{\rm pr}t}\right) \;, \\ V_{\rm pu} &= \frac{\hbar\Omega_{\rm pu}}{2}\left(|{\rm a}\rangle\langle{\rm c}|{\rm e}^{{\rm i}\omega_{\rm pu}t} + |{\rm c}\rangle\langle{\rm a}|{\rm e}^{-{\rm i}\omega_{\rm pu}t}\right) \;, \end{aligned}$$

where the rotating wave approximation has been made.

The Hamiltonian can be rewritten in matrix form, equation C.10 ,

$$\mathscr{H} \;=\; \begin{pmatrix} \hbar\omega_{\rm a} & (\hbar\Omega_{\rm pr}/2)\,{\rm e}^{-{\rm i}\omega_{\rm pr}t} & (\hbar\Omega_{\rm pu}/2)\,{\rm e}^{-{\rm i}\omega_{\rm pu}t} \\ (\hbar\Omega_{\rm pr}/2)\,{\rm e}^{{\rm i}\omega_{\rm pr}t} & \hbar\omega_{\rm b} & 0 \\ (\hbar\Omega_{\rm pu}/2)\,{\rm e}^{{\rm i}\omega_{\rm pu}t} & 0 & \hbar\omega_{\rm c} \end{pmatrix} \;.$$

The density matrix for the three-level system is given by equation C.11 ,

$$\rho \;=\; \begin{pmatrix} \rho_{\rm aa} & \rho_{\rm ab} & \rho_{\rm ac} \\ \rho_{\rm ba} & \rho_{\rm bb} & \rho_{\rm bc} \\ \rho_{\rm ca} & \rho_{\rm cb} & \rho_{\rm cc} \end{pmatrix} \;.$$

Using the Liouville equation (equation 2.21),

$$\dot{\rho} = \frac{\mathrm{i}}{\hbar}[\rho, \mathscr{H}] - \gamma\rho \ ,$$

the equations of motion for the populations and coherences are derived in appendix C. The equations for the populations are given by equations C.28, C.29, and C.30 on page 163 ,

$$\begin{aligned}
\dot{\rho}_{\mathrm{aa}} &= \frac{\mathrm{i}\Omega_{\mathrm{pr}}}{2}\left(\widetilde{\rho}_{\mathrm{ab}} - \widetilde{\rho}_{\mathrm{ba}}\right) + \frac{\mathrm{i}\Omega_{\mathrm{pu}}}{2}\left(\widetilde{\rho}_{\mathrm{ac}} - \widetilde{\rho}_{\mathrm{ca}}\right) - \Gamma_{\mathrm{a}}\rho_{\mathrm{aa}} \ , \\
\dot{\rho}_{\mathrm{bb}} &= \frac{\mathrm{i}\Omega_{\mathrm{pr}}}{2}\left(\widetilde{\rho}_{\mathrm{ba}} - \widetilde{\rho}_{\mathrm{ab}}\right) - \Gamma_{\mathrm{b}}\rho_{\mathrm{bb}} + \frac{\Gamma_{\mathrm{a}}}{2}\rho_{\mathrm{aa}} \ , \\
\dot{\rho}_{\mathrm{cc}} &= \frac{\mathrm{i}\Omega_{\mathrm{pu}}}{2}\left(\widetilde{\rho}_{\mathrm{ca}} - \widetilde{\rho}_{\mathrm{ac}}\right) - \Gamma_{\mathrm{c}}\rho_{\mathrm{cc}} + \frac{\Gamma_{\mathrm{a}}}{2}\rho_{\mathrm{aa}} \ .
\end{aligned}$$

Similarly the equations of motion for the coherences are given by equations C.33, C.34, and C.35 on page 164 ,

$$\begin{aligned}
\dot{\widetilde{\rho}}_{\mathrm{ab}} &= -\left(\gamma_{\mathrm{ab}} - \mathrm{i}\delta_{\mathrm{pr}}\right)\widetilde{\rho}_{\mathrm{ab}} + \frac{\mathrm{i}\Omega_{\mathrm{pr}}}{2}\left(\rho_{\mathrm{aa}} - \rho_{\mathrm{bb}}\right) \\
&\quad - \frac{\mathrm{i}\Omega_{\mathrm{pu}}}{2}\widetilde{\rho}_{\mathrm{cb}} \ , \\
\dot{\widetilde{\rho}}_{\mathrm{ac}} &= -\left(\gamma_{\mathrm{ac}} - \mathrm{i}\delta_{\mathrm{pu}}\right)\widetilde{\rho}_{\mathrm{ac}} + \frac{\mathrm{i}\Omega_{\mathrm{pu}}}{2}\left(\rho_{\mathrm{aa}} - \rho_{\mathrm{cc}}\right) \\
&\quad - \frac{\mathrm{i}\Omega_{\mathrm{pr}}}{2}\widetilde{\rho}_{\mathrm{bc}} \ , \\
\dot{\widetilde{\rho}}_{\mathrm{cb}} &= -\left(\gamma_{\mathrm{cb}} - \mathrm{i}\left(\delta_{\mathrm{pr}} - \delta_{\mathrm{pu}}\right)\right)\widetilde{\rho}_{\mathrm{cb}} + \frac{\mathrm{i}\Omega_{\mathrm{pr}}}{2}\widetilde{\rho}_{\mathrm{ca}} \\
&\quad - \frac{\mathrm{i}\Omega_{\mathrm{pu}}}{2}\widetilde{\rho}_{\mathrm{ab}} \ .
\end{aligned}$$

In the steady state the rate of change of the coherences are given by,

$$\begin{aligned}
\dot{\widetilde{\rho}}_{\mathrm{ab}} &= \dot{\widetilde{\rho}}_{\mathrm{ac}} \ , \\
&= \dot{\widetilde{\rho}}_{\mathrm{cb}} \ , \\
&= 0 \ .
\end{aligned} \tag{3.13}$$

Likewise the rates of change of populations in this regime are given by,

$$\begin{aligned}
\dot{\rho}_{\mathrm{aa}} &= \dot{\rho}_{\mathrm{bb}} \ , \\
&= \dot{\rho}_{\mathrm{cc}} \ , \\
&= 0 \ .
\end{aligned} \tag{3.14}$$

Furthermore, in the steady state population will be trapped in the non-coupling state. In the case of EIT, where $\Omega_{\rm pu} \gg \Omega_{\rm pr}$, the dark state, $|{\rm NC}\rangle$ is equivalent to the ground state of the probe transition, $|{\rm b}\rangle$. Hence,

$$\begin{aligned} \rho_{\rm aa} &\simeq \rho_{\rm cc} \ , \\ &\simeq 0 \ , \end{aligned} \tag{3.15}$$

$$\rho_{\rm bb} \simeq 1 \ . \tag{3.16}$$

Substituting from equations 3.13, 3.15, and 3.16 into the equations of motion for the coherences (equations C.33, C.34, and C.35) leads to

$$\frac{{\rm i}\Omega_{\rm pu}}{2}\widetilde{\rho}_{\rm cb} \simeq -\left(\gamma_{\rm ab} - {\rm i}\delta_{\rm pr}\right)\widetilde{\rho}_{\rm ab} - \frac{{\rm i}\Omega_{\rm pr}}{2} \ , \tag{3.17}$$

$$\frac{{\rm i}\Omega_{\rm pr}}{2}\widetilde{\rho}_{\rm bc} \simeq -\left(\gamma_{\rm ac} - {\rm i}\delta_{\rm pu}\right)\widetilde{\rho}_{\rm ac} \ , \tag{3.18}$$

$$\frac{{\rm i}\Omega_{\rm pu}}{2}\widetilde{\rho}_{\rm ab} \simeq -\left(\gamma_{\rm cb} - {\rm i}\left(\delta_{\rm pr} - \delta_{\rm pu}\right)\right)\widetilde{\rho}_{\rm cb} + \frac{{\rm i}\Omega_{\rm pr}}{2}\widetilde{\rho}_{\rm ca} \ . \tag{3.19}$$

In the case that the populations of two levels is small, then the coherence between those two levels will be correspondingly small. This in conjunction with the fact that $\Omega_{\rm pr} \ll \Omega_{\rm pu}$, then the term $({\rm i}\Omega_{\rm pr}/2)\,\widetilde{\rho}_{\rm ca}$ in equation 3.19 can be neglected.

The absorption and dispersion experienced by a probe beam scanned across the transition $|{\rm b}\rangle \rightarrow |{\rm a}\rangle$ is proportional to the imaginary and real components of the coherence $\widetilde{\rho}_{\rm ab}$, as shown in chapter 2. To determine $\widetilde{\rho}_{\rm ab}$, substitute equation 3.17 into equation 3.19 multiplied by ${\rm i}\Omega_{\rm pu}/2$. This leads to,

$$-\left(\frac{\Omega_{\rm pu}}{2}\right)^2\widetilde{\rho}_{\rm ab} = \left(\gamma_{\rm cb} - {\rm i}\left(\delta_{\rm pr} - \delta_{\rm pu}\right)\right)\left(\frac{{\rm i}\Omega_{\rm pr}}{2} + \left(\gamma_{\rm ab} - {\rm i}\delta_{\rm pr}\right)\widetilde{\rho}_{\rm ab}\right) \ , \tag{3.20}$$

$$\Longrightarrow \quad \widetilde{\rho}_{\rm ab}\left(\frac{\left(\Omega_{\rm pu}/2\right)^2}{\gamma_{\rm cb} - {\rm i}\left(\delta_{\rm pr} - \delta_{\rm pu}\right)} + \left(\gamma_{\rm ab} - {\rm i}\delta_{\rm pr}\right)\right) = -\frac{{\rm i}\Omega_{\rm pr}}{2} \ , \tag{3.21}$$

$$\therefore \quad \widetilde{\rho}_{\rm ab} = -\frac{{\rm i}\Omega_{\rm pr}}{2}\cdot 1 \Bigg/ \left(\left(\gamma_{\rm ab} - {\rm i}\delta_{\rm pr}\right) + \frac{\left(\Omega_{\rm pu}/2\right)^2}{\gamma_{\rm cb} - {\rm i}\left(\delta_{\rm pr} - \delta_{\rm pu}\right)}\right) \ . \tag{3.22}$$

From equation 2.64 on page 20 the complex refractive index of the medium is given by

$$\chi = -2 \frac{N \mathrm{d}_{\mathrm{ba}}^2}{\epsilon_0 \hbar \Omega_{\mathrm{pr}}} \widetilde{\rho}_{\mathrm{ab}} . \tag{3.23}$$

Utilising the Bloch vector notation (equation 2.65 on page 20 and equations 2.85, 2.86 on page 21 and equation 2.94 on page 23) the absorption coefficient, α, and dispersion, n_{R}, can be derived,

$$\alpha = -2 \frac{N \mathrm{d}_{\mathrm{ba}}^2}{\epsilon_0 \hbar} k_{\mathrm{pr}} \frac{v}{\Omega_{\mathrm{pr}}} , \tag{3.24}$$

$$n_{\mathrm{R}} = 1 - \frac{N \mathrm{d}_{\mathrm{ba}}^2}{\epsilon_0 \hbar} \cdot \frac{u}{\Omega_{\mathrm{pr}}} . \tag{3.25}$$

In this case,

$$\frac{u}{\Omega_{\mathrm{pr}}} = \mathrm{Re} \left\{ -\frac{\mathrm{i}}{2} \cdot 1 \Bigg/ \left((\gamma_{\mathrm{ab}} - \mathrm{i}\delta_{\mathrm{pr}}) + \frac{(\Omega_{\mathrm{pu}}/2)^2}{\gamma_{\mathrm{cb}} - \mathrm{i}\,(\delta_{\mathrm{pr}} - \delta_{\mathrm{pu}})} \right) \right\} , \tag{3.26}$$

$$\frac{v}{\Omega_{\mathrm{pr}}} = \mathrm{Im} \left\{ -\frac{\mathrm{i}}{2} \cdot 1 \Bigg/ \left((\gamma_{\mathrm{ab}} - \mathrm{i}\delta_{\mathrm{pr}}) + \frac{(\Omega_{\mathrm{pu}}/2)^2}{\gamma_{\mathrm{cb}} - \mathrm{i}\,(\delta_{\mathrm{pr}} - \delta_{\mathrm{pu}})} \right) \right\} . \tag{3.27}$$

Plots are made of the components of the Bloch vector as given in equations 3.26 and 3.27 . Fig. 3.3 shows $v/(\Omega_{\mathrm{pr}}/\gamma_{\mathrm{ab}})$ and $u/(\Omega_{\mathrm{pr}}/\gamma_{\mathrm{ab}})$ as a functions of $\Omega_{\mathrm{pu}}/\gamma_{\mathrm{ab}}$ and $\delta_{\mathrm{pr}}/\gamma_{\mathrm{ab}}$, where $\gamma_{\mathrm{cb}}/\gamma_{\mathrm{ab}} = 10^{-6}$, and $\delta_{\mathrm{pu}} = 0$.

Fig. 3.4 shows $v/(\Omega_{\mathrm{pr}}/\gamma_{\mathrm{ab}})$ and $v/(\Omega_{\mathrm{pr}}/\gamma_{\mathrm{ab}})$ as functions of $\Omega_{\mathrm{pu}}/\gamma_{\mathrm{ab}}$ and $\delta_{\mathrm{pr}}/\gamma_{\mathrm{ab}}$, where $\gamma_{\mathrm{cb}}/\gamma_{\mathrm{ab}} = 10^{-6}$, and $\delta_{\mathrm{pu}} = 0$.

As can be seen clearly from Fig. 3.3 (iii) and (iv), the initial increase in the Rabi frequency of the pump field from 0 causes the appearance of the induced transparency and with it the concomitant modification to the dispersion profile. Fig. 3.3 (i) and (ii) show that the continued escalation of the Rabi frequency of the pump beam lead the amplitude of the modification, to both u and v, to saturate. As the amplitude increases the width of the resonance does too. Once the amplitude has saturated, at $v = 0$ and $u = \pm 0.5$ respectively, continued inflation of the Rabi frequency of the pump simply broadens the EIT resonance.

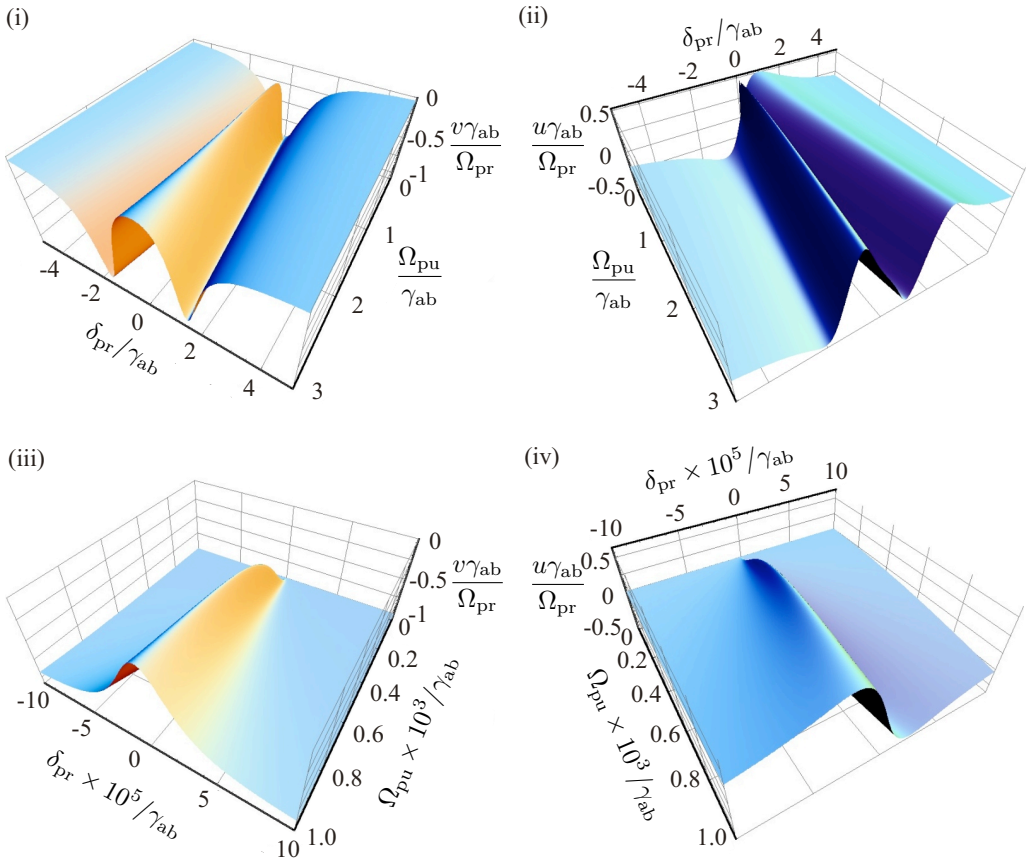

Figure 3.3: Three dimensional plots of the Bloch vector components (i) v and (ii) u, as a function of the Rabi frequency of the pump, Ω_{pu} and the detuning of the probe field from resonance, δ_{pr}. Both Ω_{pu} and δ_{pr} are plotted in units of the probe transition coherence decay rate, γ_{ab}. The ground state coherence decay rate, γ_{cb} is set to 10^{-6} γ_{ab}, and the pump beam detuning, $\delta_{pu} = 0$. (i) and (ii) show the progression of v and u respectively until the amplitude of the EIT features saturate at 0 and ± 0.5 respectively. Further increase in Ω_{pu} leads solely to broadening of the feature. (iii) and (iv) show the initial growth of the EIT feature in the narrow central region of the probe transition for small Rabi frequencies of the pump beam.

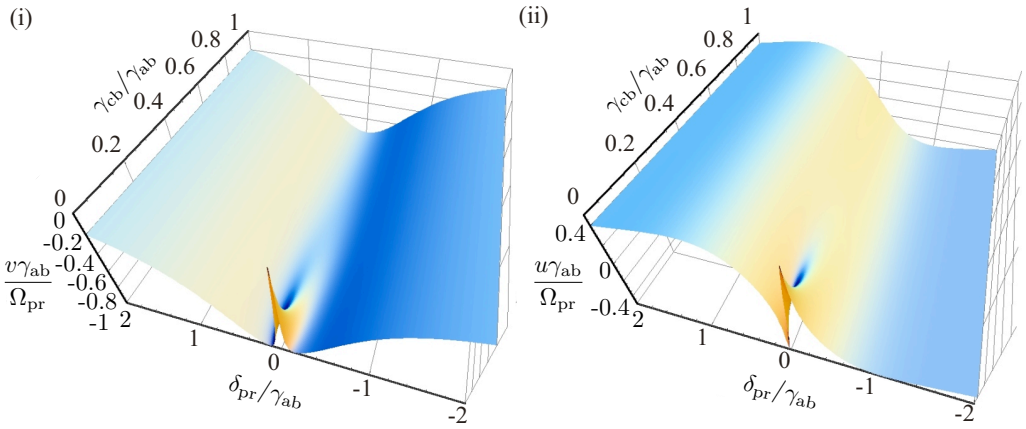

Figure 3.4: Three dimensional plots of the Bloch vector components (i) v and (ii) u, as a function of the ground state coherence decay rate, γ_{cb} and the detuning of the probe field from resonance, δ_{pr}. Both γ_{cb} and δ_{pr} are plotted in units of the probe transition coherence decay rate, γ_{ab}. The pump field has a Rabi frequency, $\Omega_{pu} = 0.3 \times \gamma_{ab}$, and is on resonance, $\delta_{pu} = 0$. As can be clearly seen in both plots an increase in the decay rate of the ground state coherence leads to significant reduction in the amplitude of the EIT resonance, such that when $\gamma_{ab} \simeq \Omega_{pu}$, the EIT signal is indistinguishable from the background.

Fig. 3.4 (i) and (ii) show $v/(\Omega_{pr}/\gamma_{ab})$ and $u/(\Omega_{pr}/\gamma_{ab})$ respectively as a function of γ_{cb}/γ_{ab} and δ_{pr}/γ_{ab}, where $\Omega_{pu}/\gamma_{ab} = 0.3$, and $\delta_{pu} = 0$. As is clearly shown in the two figures, the EIT feature is at its narrowest and largest amplitude when the coherence decay rate between the ground states is minimized. As the ground state coherence decay rate approaches the value of the Rabi frequency of the pump the EIT signal becomes indistinguishable from the background.

3.5 Line Broadening Mechanisms

It is apparent that in the case of a weak probe, the variables affecting the line width and amplitude of the EIT resonance are the Rabi frequency of the pump field, the lifetime of the coherences of the probe transition and the lifetime of the coherences between the ground states[1]. It is trivial to control the Rabi frequency of the pump simply by adjusting its intensity. The decay rates of the coherences have a minimum value derived from the natural line width of the ground and excited states, equation C.15. While it is not possible to increase the lifetimes of these states beyond the natural line width, it is possible to reduce their lifetimes through collisions with atoms and cell walls.

This section will concentrate on other mechanisms which either modify the width or shape of the EIT resonances. These include: the magnetic field; the relative directions of propagation of pump and probe beam; the line width of the lasers used to provide the pump and probe beam; the finite extent of the pump and probe beams and the intensity profile of the pump and probe beams.

In order to produce a theoretical model of EIT that would reproduce the experimentally observed spectra further measures have to be taken. EIT on the Rb D_2 line is not simply two fields interacting with three levels; there are in fact 60 different Zeeman sub-levels across both isotopes. A theoretical model taking account of all of the levels and the optical pumping between them is beyond the scope of this work. Doppler broadening of the hyperfine transitions is also relevant as it means that at any detuning of the pump beam within the Doppler-broadened hyperfine resonances will lead to the pump beam being resonant with different hyperfine transitions for different velocity classes of atoms.

[1] Collisional broadening can lead to broader resonances when it limits the relaxation rate of the atoms. This is not a factor in the work presented in this thesis. If the temperature or density of the Rb atoms was increased, or if a buffer gas was introduced, collisional broadening could become significant.

3.5.1 Magnetic Field Sensitivity

Three-level systems can be between three different hyperfine states or between Zeeman sublevels within two hyperfine states. As Zeeman levels are magnetically sensitive, it follows that resonances with Zeeman levels are subject to magnetic broadening in an inhomogeneous magnetic field.

Zeeman Effect

Every hyperfine state F has $2F + 1$ Zeeman sub-levels, denoted m_F, where $-F \leqslant m_F \leqslant F$. These Zeeman sub-levels are given by the projection of the total angular momentum F onto an external magnetic field $\mathbf{B}$.

The energy shift due to the Zeeman effect is ΔE_{Z}. Fig. 3.5 shows a Λ system with two ground states that are Zeeman sublevels of the same hyperfine state. It follows that the energy difference between the Zeeman sub-levels varies with $\mathbf{B}$, and in the region of interest, where $\Delta E_{\mathrm{Z}} \ll \Delta E_{\mathrm{HFS}}$ (where ΔE_{HFS} is the hyperfine splitting), it can be taken to vary linearly with the magnitude of the magnetic field, B. The Zeeman shift is

$$\Delta E_{\mathrm{Z}} = g_{\mathrm{F}} \mu_{\mathrm{B}} B m_F \ . \tag{3.28}$$

g_{F} is an effective Landé g-value, given by:

$$\begin{aligned} g_{\mathrm{F}} &= g_{\mathrm{J}} \frac{F(F+1) + J(J+1) - I(I+1)}{2F(F+1)} \\ &\quad - g'_{\mathrm{I}} \frac{F(F+1) - J(J+1) + I(I+1)}{2F(F+1)} \ , \end{aligned} \tag{3.29}$$

where,

$$\begin{aligned} g_{\mathrm{J}} &= \frac{J(J+1) + L(L+1) - S(S+1)}{2J(J+1)} \\ &\quad + g_{\mathrm{S}} \frac{J(J+1) - L(L+1) + S(S+1)}{2J(J+1)} \ , \end{aligned} \tag{3.30}$$

and,

$$g_{\mathrm{S}} \simeq 2 \ , \tag{3.31}$$

$$\implies g_{\mathrm{J}} = \frac{3J(J+1) - L(L+1) + S(S+1)}{2J(J+1)} \ . \tag{3.32}$$

As $g'_{\rm I} \sim m/M$, where m is the electron mass and M is the proton mass, then $g'_{\rm I} \ll g_{\rm J}$. Hence,

$$g_{\rm F} = \frac{3J(J+1) - L(L+1) + S(S+1)}{2J(J+1)} \times \frac{F(F+1) + J(J+1) - I(I+1)}{2F(F+1)} \,. \tag{3.33}$$

The notation used above is following that used in *Elementary Atomic Structure*, [61].

The values of $g_{\rm F}$ are calculated for all of the hyperfine states of the D-lines of ^{85}Rb and ^{87}Rb, and are shown in table 3.1 and 3.2, respectively. There is no $g_{\rm F}$ for $F = 0$.

Term	F			
	1	2	3	4
$^2S_{1/2}$		$-1/3$	$1/3$	
$^2P_{1/2}$		$-1/9$	$1/9$	
$^2P_{3/2}$	-1	$1/9$	$7/18$	$1/2$

Table 3.1: $g_{\rm F}$ for the hyperfine states of ^{85}Rb.

Term	F		
	1	2	3
$^2S_{1/2}$	$-1/2$	$1/2$	
$^2P_{1/2}$	$-1/6$	$1/6$	
$^2P_{3/2}$	$2/3$	$2/3$	$2/3$

Table 3.2: $g_{\rm F}$ for the hyperfine states of ^{87}Rb.

In the following chapters a Λ system made up of σ_+ and σ_- beams with the states $|\mathrm{b}\rangle$ and $|\mathrm{c}\rangle$ being $|F,\ m_F = -1\rangle$ and $|F,\ m_F = +1\rangle$ will be considered.

The linear frequency shift in the position of such a resonance is calculated and shown in tables 3.3 and 3.4 .

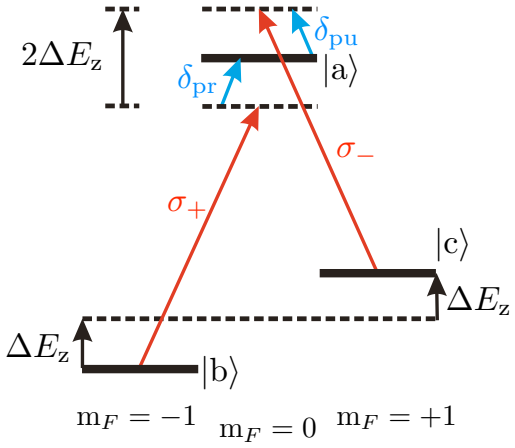

Figure 3.5: ΔE_z is the magnitude of the shift of the levels due to the Zeeman effect, in the absence of the B-field both σ_+ and σ_- would be on resonance with the states shown.

Term	F			
	1	2	3	4
$^2S_{1/2}$		−0.47	+0.47	
$^2P_{1/2}$		−0.16	+0.16	
$^2P_{3/2}$	− 1.4	+0.16	+0.54	+0.7

Table 3.3: Ratio of the Zeeman shift to m_F (MHz/G) for the hyperfine states of ^{85}Rb.

Term	F		
	1	2	3
$^2S_{1/2}$	−0.7	+0.7	
$^2P_{1/2}$	−0.23	+0.23	
$^2P_{3/2}$	+0.93	+0.93	+0.93

Table 3.4: Ratio of the Zeeman shift to m_F (MHz/G) for the hyperfine states of ^{87}Rb.

Magnetic Field Broadening

If the levels in an EIT system are magnetically sensitive, then it follows that a non-uniform magnetic field can cause position-dependent shifts in the frequency of the resonance.

Specifically, consider the case of a Λ system where both ground states are different Zeeman sub-levels of the same hyperfine level (see Fig. 3.5).

Any non-uniformity in magnetic field, $\Delta\mathbf{B}$ along the axis of the pump and probe beam, will lead to a broadening of any feature by an amount $\Delta\nu$. From equation 3.28,

$$\Delta\nu \;=\; \frac{g_{\mathrm{F}}\mu_{\mathrm{B}}\Delta B\Delta m_F}{h}\;, \tag{3.34}$$

where Δm_F is the difference in m_F values between the ground states.

3.5.2 Probe and Pump Beam Crossing Angle

When pump and probe fields were discussed previously it was in relation to saturation spectroscopy, § 2.6.1 on page 39, and counter-propagating beams were required. In order to determine the appropriate orientation for pump and probe beams for EIT in a Λ system the following analysis is required.

Consider a scheme in which a pump and a probe beam propagate at an angle θ to one another, Fig. 3.6. In addition consider an atom propagating at an angle α to the bisector of the pump and probe, with a velocity, $\mathbf{v}$. The atom's velocity can be resolved into two components, $\mathbf{v}_{\parallel}$, parallel to the bisector of the pump and probe and $\mathbf{v}_{\perp}$, perpendicular to the bisector. This causes a change in the detuning of both the probe and pump from the resonances, $|\mathrm{b}\rangle \rightarrow |\mathrm{a}\rangle$ and $|\mathrm{c}\rangle \rightarrow |\mathrm{a}\rangle$, respectively,

$$\delta_{\mathrm{pr}} \;\rightarrow\; \delta_{\mathrm{pr}} - \boldsymbol{k}_{\mathrm{pr}}\cdot\mathbf{v}\;, \tag{3.35}$$

$$\delta_{\mathrm{pu}} \;\rightarrow\; \delta_{\mathrm{pu}} - \boldsymbol{k}_{\mathrm{pu}}\cdot\mathbf{v}\;. \tag{3.36}$$

Thus the coherence, $\widetilde{\rho}_{\mathrm{ab}}$ (equation 3.22) that leads to the probe absorption and

dispersion, becomes,

$$\widetilde{\rho}_{\rm ab} = \frac{-{\rm i}\Omega_{\rm pr}}{2} \times \left((\gamma_{\rm ab} - {\rm i}\,(\delta_{\rm pr} - \boldsymbol{k}_{\rm pr}\cdot\mathbf{v})) + \frac{(\Omega_{\rm pu}/2)^2}{\gamma_{\rm cb} - {\rm i}\,(\delta_{\rm pr} - \delta_{\rm pu} + \boldsymbol{k}_{\rm pu}\cdot\mathbf{v} - \boldsymbol{k}_{\rm pr}\cdot\mathbf{v})} \right)^{-1} . \tag{3.37}$$

A shift in frequency of the two-photon resonance, $\delta_{\mathbf{v}}$, will result. For a Λ system this will take the form,

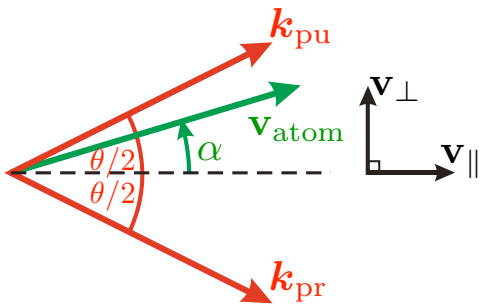

Figure 3.6: The diagram shows the crossing angle of the pump and probe beams, θ. The direction of propagation of the atoms in the medium is given by α. The reference coordinates are $\mathbf{v}_{\parallel}$, the bisector of the pump and probe beams, and $\mathbf{v}_{\perp}$ the perpendicular to the bisector of the pump and probe beams.

$$\delta_{\mathbf{v}} = (\boldsymbol{k}_{\rm pu} - \boldsymbol{k}_{\rm pr})\cdot\mathbf{v} , \tag{3.38}$$

$$= k_{\rm pu}{\rm v}\cos\left(\frac{\theta}{2} - \alpha\right) - k_{\rm pr}{\rm v}\cos\left(\frac{\theta}{2} + \alpha\right) ,$$

$$= \left[k_{\rm pu}\left(\cos\frac{\theta}{2}\cos\alpha + \sin\frac{\theta}{2}\sin\alpha\right) - k_{\rm pr}\left(\cos\frac{\theta}{2}\cos\alpha - \sin\frac{\theta}{2}\sin\alpha\right)\right]{\rm v} . \tag{3.39}$$

$$\text{Re-writing}\quad k_{\rm pu} = k_{\rm pr} + \delta k , \tag{3.40}$$

$$\text{then}\quad \delta_{\mathbf{v}} = \left[2k_{\rm pr}\sin\frac{\theta}{2}\sin\alpha + \delta k\cos\left(\frac{\theta}{2} - \alpha\right)\right]{\rm v} . \tag{3.41}$$

For a Λ system where both ground states are Zeeman sub-levels of the same hyperfine state, $\delta k_{\rm pr}$ is given by the Zeeman splitting. In the case of the Rb D_2 line, $k_{\rm pr} \simeq 8\times10^6$ m^{-1}. The Zeeman splitting between the two Λ groundstates

in the hyperfine state $F = 1$ of ^{87}Rb for a magnetic field of 1 G is 1.40 MHz (see table 3.4 on page 57) this gives $\delta k = 29.3 \times 10^{-3}$ m^{-1} , leading to:

$$\frac{\delta k}{k_{\rm pr}} \simeq 10^{-9} \ . \tag{3.42}$$

Resolving the velocity of the atom into its two components, $\mathrm{v}_{\parallel}$ and $\mathrm{v}_{\perp}$, where,

$$\mathrm{v}_{\parallel} = |\mathbf{v}| \cos\alpha \ , \tag{3.43}$$

$$\mathrm{v}_{\perp} = |\mathbf{v}| \sin\alpha \ . \tag{3.44}$$

In the case that $\delta k \ll k_{\rm pr}$, and by considering the velocity in terms the two perpendicular components equation 3.41 reduces to,

$$\delta_{\mathbf{v}} = 2k_{\rm pr} \sin(\theta/2)\mathrm{v}_{\perp} \ . \tag{3.45}$$

The single-photon detuning due to the Doppler shift of the probe is given by,

$$-\boldsymbol{k}_{\rm pr} \cdot \mathbf{v} = -k_{\rm pr}\mathrm{v}\cos\left(\frac{\theta}{2} + \alpha\right) \ , \tag{3.46}$$

$$= -k_{\rm pr}\mathrm{v}_{\rm pr} \ . \tag{3.47}$$

$\mathrm{v}_{\rm pr}$ is the component of the atom's velocity parallel to $\boldsymbol{k}_{\rm pr}$.

It follows that equation 3.37 can be written,

$$\widetilde{\rho}_{\rm ab} = -\frac{\mathrm{i}\Omega_{\rm pr}}{2} \times \left((\gamma_{\rm ab} - \mathrm{i}\,(\delta_{\rm pr} - k_{\rm pr}\mathrm{v}_{\rm pr})) + \frac{(\Omega_{\rm pu}/2)^2}{\gamma_{\rm cb} - \mathrm{i}\,(\delta_{\rm pr} - \delta_{\rm pu} + 2k_{\rm pr}\sin(\theta/2)\mathrm{v}_{\perp})} \right)^{-1} \ . \tag{3.48}$$

In a vapour cell the velocity distribution of the atoms is homogeneous and isotropic and is given by the Maxwellian distribution. From § 2.3.4 and equation 2.96 on page 24, the Maxwellian velocity distribution is given by,

$$N\left(\mathrm{v_z}\right)\mathrm{dv_z} = \frac{N}{\sqrt{\pi}} \cdot \sqrt{\frac{m}{2\mathrm{k_B}T}}\, \exp\left[-\left(\mathrm{v_z}\sqrt{\frac{m}{2\mathrm{k_B}T}} \right)^2 \right] \mathrm{dv_z} \ .$$

v_z is the velocity in one dimension. As the velocity is isotropic in the vapour cell, then the distribution of v_z is the same as the distribution of $\mathrm{v}_{\perp}$ and $\mathrm{v}_{\rm pr}$.

It follows that the absorption coefficient of the medium is given by,

$$\alpha \propto \int_{-\infty}^{\infty}\int_{-\infty}^{\infty} \mathrm{Im}\left\{\widetilde{\rho}_{\rm ab}\right\}(\mathrm{v}_{\rm pr}, \mathrm{v}_{\perp}) N\left(\mathrm{v}_{\rm pr}\right) N\left(\mathrm{v}_{\perp}\right) \mathrm{dv}_{\rm pr}\mathrm{dv}_{\perp} \ . \tag{3.49}$$

Using *Mathematica*, the absorption of such a medium has been calculated. The normalized absorption coefficient is given by,

$$\alpha_{\text{norm}} = \frac{\alpha}{\alpha\left(\delta_{\text{pr}} = 0,\ \Omega_{\text{pu}} = 0\right)} . \tag{3.50}$$

A plot of the line-centre normalized absorption coefficient is shown in Fig. 3.7 . As can be seen the EIT resonance dies away rapidly as the pump and probe move away from copropagating. As the temperature of the atomic ensemble increases, so does the rate at which the amplitude of the EIT resonance dies away with increasing angle between the pump and probe.

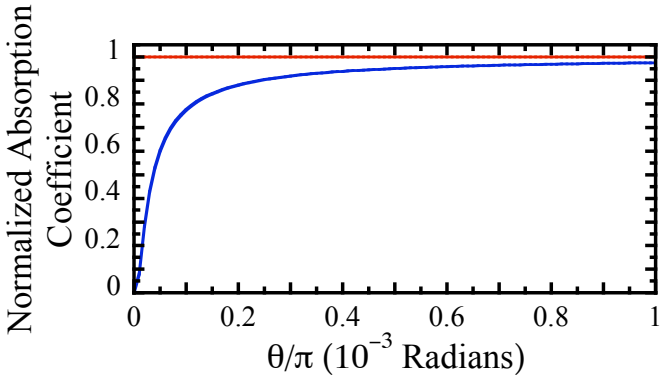

Figure 3.7: The normalized absorption coefficient for a Λ system is plotted as a function of angle between the pump and probe beam from $\theta = 0$ to $\theta = 10^{-3}\pi$. The red line shows the absorption for $\Omega_{\text{pu}} = 0$, whereas the blue line shows the absorption for $\Omega_{\text{pu}} = 0.4\gamma_{\text{ab}}$. The velocity distribution of the atomic ensemble is that of ^{87}Rb at room temperature, 293 K. For the purpose of this plot $\delta_{\text{pr}} = 0$, $\delta_{\text{pu}} = 0$, and $\gamma_{\text{cb}} = 10^{-6}\gamma_{\text{ab}}$.

An experimental verification of this has been provided by Carvalho *et al.*, [62]. Ideally in the three-level Λ and V type systems, the pump and probe should be perfectly co-propagating to cancel the Doppler broadening of the two-photon resonance (due to component of the atoms' velocity perpendicular to the bisector of the pump and probe beams) to as high a degree as possible.

3.5.3 Laser Line Width

Including the line widths of the lasers used in measuring EIT resonances (probe and pump) would lead to the increased rate of decay of atomic coherences, [63]. This would have the effect of broadening and reducing the amplitude of the EIT resonances as seen in Fig. 3.4.

This effect can be cancelled in a Λ system if there is a critical cross-correlation between the pump and probe, [64]. The critical cross-correlation causes any laser jitter to cancel in its effect on the Λ-system. This is often achieved by phase locking the pump and probe laser together, [20]. It is also possible to injection lock one laser to another by modulating the current to one laser, [65]. This induces sidebands on the output of the first laser. One of these sidebands is injected into the second laser. The output of the second laser is phase locked to the first and at a frequency separation given by the modulation frequency of the laser current.

An alternative method is to use one laser to provide both pump and probe beams. Any frequency offset between the pump and probe field can be provided by an optical element such as an acousto-optic modulator. Thus it is possible to measure resonances many orders of magnitude narrower than the line width of the laser.

3.5.4 Transit-Time Broadening

Atoms with a non-zero velocity perpendicular to the direction of propagation of the pump and probe beams will traverse the pump and probe beams in a finite time. In the atoms's frame of reference this takes the form of the pump and probe beams comprising of finite pulses as opposed to continuous wave laser beams. Any finite time pulse has a spread in frequency about the mean frequency of the continuous wave beam. The shorter the pulse the greater the spread in frequency. This leads to broadening of any spectral features, and is referred to as transit-time broadening.

The case in which the EIT resonance is transit time broadened is addressed by Thomas and Quivers Jr., [66]. They consider the scheme in which the pump and probe beams have a Gaussian intensity profile. When the groundstate

lifetime is much longer than the transit time of the atoms through the beams; the excited state lifetime is much less than the transit time of the atoms through the beam; and where the pump and probe powers are small enough that they do not contribute to the broadening, then the expected line shape is a cusp function, with a FWHM, Γ_{EIT}, given by,

$$\Gamma_{\mathrm{EIT}} = \frac{2\sqrt{2}\ \ln 2\ \mathrm{v}}{d}\ . \tag{3.51}$$

d is the 1/e beam diameter and v is the thermal speed of the atoms,

$$\mathrm{v} \ = \ \sqrt{\frac{2\mathrm{k_B}T}{m}}\ , \tag{3.52}$$

$\mathrm{k_B}$ is the Boltzmann constant, T is the temperature of the atoms and m is the atomic mass. A cusp function being a back-to-back exponential of the general form,

$$\exp\left(-\left|\frac{\omega-\omega_0}{\omega_\Delta}\right|\right)\ , \tag{3.53}$$

where ω_Δ is the 1/e half-width [2], ω is the frequency and ω_0 is the frequency of the centre of the resonance.

An experimental study of this has been made by Knappe *et al.*, [67]. Knappe *et al.* show that for narrow beam the cusp line shape gives a better fit than the standard Lorentzian model. However at line centre the cusp model does not fit the data, this is explained as being due to other broadening effects. As the width of the beam is increased, the cusp model becomes a less good fit, whilst the Lorenzian model accurately describes the resonance line shape.

3.5.5 Beam Profile Effect on Line Shape

In the previous subsection the case of transit-time broadening was addressed for beams with Gaussian intensity profiles. In the work that is presented in this thesis, the profiles of the probe and pump beams can not always be described by a Gaussian function. The pump and probe beams are expected to have a Gaussian profile when an optical fibre patchcord is used to ensure that they are overlapped. In all other cases the profile will not necessarily be uniform, nor

[2] For a cusp function the 1/e half width is equal to FWHM/(2 ln 2) .

Gaussian. This is due to the optical elements that the beams have traversed on their way to the vapour cell.

Taĭchenachev et al., [68], consider the effect of different beam profiles. The regime considered by Taĭchenachev *et al.* is that in which the relaxation rate of the atoms, $\Gamma_{\rm L}$, is much greater than the diffusion rate of the atoms through the beams. For a buffer gas cell,

$$\Gamma_{\rm L} \gg \frac{D}{r_0^2} \ , \tag{3.54}$$

and no for no buffer gas, where

$$\Gamma_{\rm L} \gg \frac{\rm v}{r_0} \ . \tag{3.55}$$

D is the diffusion constant, v is defined in equation 3.52 , and r_0 is the 1/e radius of the beam.

The two contrasting beam profiles are of the form,

$$I \ = \ I_0 \ f\left(\frac{r}{r_0}\right) \ , \tag{3.56}$$

where there is the standard Gaussian,

$$f\left(\frac{r}{r_0}\right) \ = \ {\rm e}^{-(r/r_0)^2} \ , \tag{3.57}$$

and a step-like profile,

$$f\left(\frac{r}{r_0}\right) \ = \ 1, \quad r \leqslant r_0 \ ; \tag{3.58}$$

$$= \ 0, \quad r_0 \leqslant r \ . \tag{3.59}$$

The FWHM of the EIT features for Gaussian, $\Gamma_{\rm G}$, and step-like, $\Gamma_{\rm STEP}$, beams are given by,

$$\Gamma_{\rm G} \ \simeq \ 0.86 Z_0 \gamma_{\rm cb} \ , \tag{3.60}$$

$$\Gamma_{\rm STEP} \ \simeq \ 2 Z_0 \gamma_{\rm cb} \ , \tag{3.61}$$

respectively. $\gamma_{\rm cb}$ is the decay rate of coherence between the two lower states of the Λ system, and

$$Z_0 \ = \ 2 \cdot \frac{\Omega_{\rm pr}^2 + \Omega_{\rm pu}^2}{\Gamma_{\rm a}^2} \cdot \frac{1}{\gamma_{\rm cb}/\Gamma_{\rm a}} \ , \tag{3.62}$$

$$= \ 2 \cdot \frac{\Omega_{\rm pr}^2 + \Omega_{\rm pu}^2}{\Gamma_{\rm a} \gamma_{\rm cb}} \ , \tag{3.63}$$

Substituting equation 3.63 into equations 3.60 and 3.61 leads to,

$$\Gamma_{\mathrm{G}} \simeq 1.72 \cdot \frac{\Omega_{\mathrm{pr}}^2 + \Omega_{\mathrm{pu}}^2}{\Gamma_{\mathrm{a}}} , \tag{3.64}$$

$$\Gamma_{\mathrm{STEP}} \simeq 4 \cdot \frac{\Omega_{\mathrm{pr}}^2 + \Omega_{\mathrm{pu}}^2}{\Gamma_{\mathrm{a}}} , \tag{3.65}$$

The step-like beam profile leads to the standard Lorentzian line shape. The Gaussian beam profile leads to a more complicated line shape, $\mathcal{R}_{\mathrm{G}}$, which in the limit that,

$$Z_0 \gg 1 , \tag{3.66}$$

$$\text{is given by} \quad \mathcal{R}_{\mathrm{G}} = 1 - \frac{\Delta}{Z_0} \cdot \arctan\left(\frac{Z_0}{\Delta}\right) , \tag{3.67}$$

where Δ is the two-photon detuning normalized to the ground state coherence decay rate, $(\delta_{\mathrm{pr}} - \delta_{\mathrm{pu}})/\gamma_{\mathrm{cb}}$.

3.5.6 Doppler Broadening Effect on EIT Line Width

Javan et al., [69], have theoretically studied the effect of Doppler-broadening of a medium on the EIT line width. They find an explicit expression for the FWHM of an EIT resonance, Γ_{EIT}, in a Doppler-broadened medium.

$$\Gamma_{\mathrm{EIT}}^2 = \frac{\gamma_{\mathrm{cb}}\Omega_{\mathrm{pu}}^2}{\Gamma_{\mathrm{a}}} \cdot (1+x)\left(1 + \sqrt{1 + \frac{4x}{(1+x)^2}}\right) , \tag{3.68}$$

$$\text{where,} \quad x = \frac{\Gamma_{\mathrm{a}}}{2\gamma_{\mathrm{cb}}} \cdot \frac{\Omega_{\mathrm{pu}}^2}{W_{\mathrm{D}}^2} . \tag{3.69}$$

W_{D} is the FWHM of the Doppler-broadened resonance, Ω_{pu} is the Rabi frequency of the pump field, Γ_{a} is the excited state decay rate, and γ_{cb} is the decay rate of the groundstate coherence. Note that this is in the regime where the probe intensity is vanishingly small. Substituting equation 3.63 into equation 3.69, for comparison with the beam profile contribution to line shape, leads to

$$x = \frac{\Gamma_{\mathrm{a}}^2}{4W_{\mathrm{D}}^2} \cdot Z_0\left(\Omega_{\mathrm{pr}} = 0\right) . \tag{3.70}$$

The two extreme limits of the model are for $x \ll 1$ and $x \gg 1$. From equation 3.70 it follows that the extremes correspond to,

$$\left(\frac{\Omega_{\rm pu}}{W_{\rm D}}\right)^2 \ll \frac{2\gamma_{\rm cb}}{\Gamma_{\rm a}} , \quad x \ll 1 ; \tag{3.71}$$

$$\left(\frac{\Omega_{\rm pu}}{W_{\rm D}}\right)^2 \gg \frac{2\gamma_{\rm cb}}{\Gamma_{\rm a}} , \quad x \gg 1 . \tag{3.72}$$

In the two extreme limits, this model gives two different functions for the width of the EIT resonance,

$$\Gamma_{\rm EIT} = \sqrt{\frac{\gamma_{\rm cb}}{\Gamma_{\rm a}}} \cdot \Omega_{\rm pu} , \quad x \ll 1 ; \tag{3.73}$$

$$= \frac{\Omega_{\rm pu}^2}{W_{\rm D}} , \quad x \gg 1 . \tag{3.74}$$

As the Rabi frequency is proportional to the square root of the beam intensity it follows that in the regime where $x \ll 1$, the width of the EIT feature increases in direct proportion to the square root of the intensity of the pump; in the regime where $x \gg 1$ the width of the EIT feature is proportional to the intensity of the pump.

3.6 Electromagnetically Induced Absorption

Electromagnetically Induced Absorption (EIA), [70, 71], is the increase in absorption of a probe beam by a medium due to the presence of a pump beam. There are four different systems in which EIA has been identified, [72, 73, 74, 75, 76]. Two mechanisms involve degenerate two-level systems. They rely on the transfer of coherence (TOC), [72, 73], and transfer of population (TOP), [72, 74], to generate the induced absorption.

EIA due to the transfer of coherence, EIA-TOC, requires that the pump and probe have different polarizations. EIA due to transfer of population, EIA-TOP, requires that the polarization of pump and probe should be the same.

The experimental work presented in the following chapters involves the use of orthogonally polarized pump and probe beams. Hence any EIA observed will be due to the transfer of coherence.

3.6.1 Transfer of Coherence

Taĭchenachev *et al.*, [77], first showed that EIA was due to TOC from the excited states to the ground states. No explanation was offered as to why there are systems where TOC takes place without resulting in EIA.

Goren *et al.*, [72, 73], clarified the conditions necessary for TOC to result in EIA. This can occur only when the pump and probe lasers have different polarizations and there is a significant pump-induced population in the excited state (for example one-sixth of the total population, [72]). The excited and ground hyperfine states must also meet the following criteria, $F_{\mathrm{e}} = F_{\mathrm{g}} + 1$ and $F_{\mathrm{g}} > 0$.

EIA-TOC requires at least two degenerate ground levels and at least two degenerate excited states — the N-system, Fig. 3.8 . Coherence builds up between the degenerate excited states. Spontaneous emission causes a transfer of coherence from the degenerate excited states to the degenerate ground states, [77]. It is the transfer of coherence that leads to the induced absorption.

In order for the coherence to build up between the excited states it is necessary to have a significant fraction of the population in the excited states. To get a significant fraction of the population in the excited states normally requires

that one of the pump transitions should be closed. In ^{85}Rb the closed transition is $5\ ^2S_{1/2}\ F = 3,\ m_F = \pm 3\ \rightarrow\ 5\ ^2P_{3/2}\ F = 4,\ m_F = \pm 4$ and in ^{87}Rb it is $5\ ^2S_{1/2}\ F = 2,\ m_F = \pm 2\ \rightarrow\ 5\ ^2P_{3/2}\ F = 3,\ m_F = \pm 3$. These closed transitions correspond to the transition $|c\rangle \rightarrow |d\rangle$ in Fig. 3.8. Similarly the transition $|b\rangle \rightarrow |a\rangle$ in Fig. 3.8 corresponds to $5\ ^2S_{1/2}\ F = 3,\ m_F = \pm 3\ \rightarrow\ 5\ ^2P_{3/2}\ F = 3,\ m_F = \pm 3$ in ^{85}Rb and $5\ ^2S_{1/2}\ F = 2,\ m_F = \pm 2\ \rightarrow\ 5\ ^2P_{3/2}\ F = 2,\ m_F = \pm 2$ in ^{87}Rb.

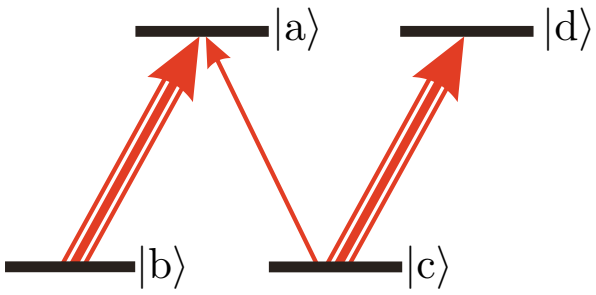

Figure 3.8: N system diagram. The two heavy red arrows show the pump transitions. The fine red arrow shows the probe transition. The difference in pump and probe polarization leads to the pump and probe being resonant with different transitions between the four states.

This normally would preclude open systems from exhibiting EIA, however open systems can exhibit EIA, [78]. An explanation of this is presented by Goren *et al.*, [72]. In this case EIA only occurs for relatively large pump Rabi frequencies. When the Rabi frequency of the pump is increased the excited state population increases and hence the excited state coherence is increased too. This leads to an increased TOC to the ground state, ultimately resulting in EIA.

Goren *et al.*, [73], carry out a full theoretical investigation of the N-system, varying the degree of TOC, and the strengths of the pump transitions[3]. It is noted that as the strength of either pump transition is reduced to zero, the spectra is consistent with what would be expected in an EIT Λ or V system. Reducing the TOC significantly reduces the predicted EIA, until for zero TOC EIT is predicted instead of EIA.

The behaviour of the N-system with TOC is also seen in the EIA spectra of the

[3]In the case that one pump beam is applied to two degenerate transitions, the strength of those transitions will not necessarily be the same. This is due to the different Clebsch-Gordan coefficients for the different transitions.

Hanle[4] configuration, as explained by Renzoni *et al.*, [80].

The recent work on optical-pumping-assisted EIT by Jiang *et al.*, [81], which shows increased transmission due to the application of a second pump field, bears many similarities to the N system involved in EIA-TOC. The most striking differences are the relative order of the pump and probe within the N system, and the significant deviation from degeneracy which prevents TOC.

3.7 Group Velocity

3.7.1 Group Velocity Derivation

In the case where an electromagnetic field does not have a single frequency, interference between the components with different frequencies will lead to a beat pattern. The rate at which the envelope of this pattern advances is known as the group velocity, $\mathrm{v_g}$, and it is given by:

$$\mathrm{v_g} = \frac{\mathrm{d}\omega}{\mathrm{d}k} \ . \tag{3.75}$$

As,

$$\omega = \frac{k\ \mathrm{c}}{n_\mathrm{R}} \ , \tag{3.76}$$

then substituting equation 3.76 into equation 3.75 leads to,

$$\begin{aligned} \mathrm{v_g} &= \frac{\mathrm{c}}{n_\mathrm{R}} + k\ \mathrm{c}\frac{\mathrm{d}\left(1/n_\mathrm{R}\right)}{\mathrm{d}n_\mathrm{R}} \cdot \frac{\mathrm{d}n_\mathrm{R}}{\mathrm{d}k} \ , \\ &= \frac{\mathrm{c}}{n_\mathrm{R}} - \frac{k\ \mathrm{c}}{n_\mathrm{R}^2} \cdot \frac{\mathrm{d}n_\mathrm{R}}{\mathrm{d}\omega} \cdot \frac{\mathrm{d}\omega}{\mathrm{d}k} \ , \end{aligned} \tag{3.77}$$

$$\implies \mathrm{v_g} + \mathrm{v_g}\frac{k\ \mathrm{c}}{n_\mathrm{R}^2} \cdot \frac{\mathrm{d}n_\mathrm{R}}{\mathrm{d}\omega} = \frac{\mathrm{c}}{n_\mathrm{R}} \ . \tag{3.78}$$

Substituting equation 3.76 into equation 3.78, leads to:

$$\mathrm{v_g} = \frac{\mathrm{c}}{n_\mathrm{R} + \omega\left(\mathrm{d}n_\mathrm{R}/\mathrm{d}\omega\right)} \ . \tag{3.79}$$

3.7.2 Lorentzian Line Shape Group Velocity

The rate of change of the real part of the refractive index with respect to frequency, $\mathrm{d}n_\mathrm{R}/\mathrm{d}\omega$, for a Lorentzian line shape can be derived from equation 2.87

[4]For an explanation of the Hanle effect see *Atomic and Laser Spectroscopy*, [79].

on page 22. In turn it is possible to determine the modification of group velocity at line centre. In the case that the probe is in the weak regime ($\Gamma_{\rm a} \gg \Omega_{\rm pr}$) then equation 2.87 becomes:

$$n_{\rm R} - 1 = -\frac{N\mathrm{d}_{\rm ba}^2}{2\epsilon_0\hbar} \cdot \frac{\delta_{\rm pr}}{\delta_{\rm pr}^2 + (\Gamma_{\rm a}/2)^2} \ . \tag{3.80}$$

Differentiating with respect to $\delta_{\rm pr}$ leads to:

$$\frac{\mathrm{d}\left(n_{\rm R} - 1\right)}{\mathrm{d}\left(\delta_{\rm pr}\right)} = \frac{N\mathrm{d}_{\rm ba}^2}{2\epsilon_0\hbar} \left[\frac{2\delta_{\rm pr}^2}{\left(\delta_{\rm pr}^2 + (\Gamma_{\rm a}/2)^2\right)^2} - \frac{1}{\delta_{\rm pr}^2 + (\Gamma_{\rm a}/2)^2} \right] \ , \tag{3.81}$$

and as,

$$\begin{aligned} \frac{\mathrm{d}(n_{\rm R} - 1)}{\mathrm{d}(\delta_{\rm pr})} &= \frac{\mathrm{d}(n_{\rm R} - 1)}{\mathrm{d}n_{\rm R}} \cdot \frac{\mathrm{d}\omega_{\rm pr}}{\mathrm{d}\delta_{\rm pr}} \cdot \frac{\mathrm{d}n_{\rm R}}{\mathrm{d}\omega_{\rm pr}} \ , & (3.82) \\ &= \frac{\mathrm{d}n_{\rm R}}{\mathrm{d}\omega_{\rm pr}} \ , & (3.83) \end{aligned}$$

where,

$$\frac{\mathrm{d}(n_{\rm R} - 1)}{\mathrm{d}n} = \frac{\mathrm{d}\omega_{\rm pr}}{\mathrm{d}\delta_{\rm pr}} \equiv 1 \ . \tag{3.84}$$

To find the frequency at which the group velocity is at its lowest, the second derivative of $n_{\rm R}$ with respect to $\omega_{\rm pr}$ has to be found and set equal to 0.

$$\begin{aligned} \frac{\mathrm{d}^2 n_{\rm R}}{\mathrm{d}\omega_{\rm pr}^2} &= \frac{N\mathrm{d}_{\rm ba}^2}{2\epsilon_0\hbar} \left[\frac{4\ \delta_{\rm pr}}{\left(\delta_{\rm pr}^2 + (\Gamma_{\rm a}/2)^2\right)^2} - \frac{8\ \delta_{\rm pr}^3}{\left(\delta_{\rm pr}^2 + (\Gamma_{\rm a}/2)^2\right)^3} \right. \\ &\qquad \left. + \frac{2\ \delta_{\rm pr}}{\left(\delta_{\rm pr}^2 + (\Gamma_{\rm a}/2)^2\right)^2} \right] \ , & (3.85) \\ &= 0 \ , & (3.86) \end{aligned}$$

$$\implies \frac{3\ \delta_{\rm pr}}{\left(\delta_{\rm pr}^2 + (\Gamma_{\rm a}/2)^2\right)^2} - \frac{4\ \delta_{\rm pr}^3}{\left(\delta_{\rm pr}^2 + (\Gamma_{\rm a}/2)^2\right)^3} = 0 \ , \tag{3.87}$$

$$\implies \delta_{\rm pr} = 0 \ , \tag{3.88}$$

$$\begin{aligned} \text{or,} \quad 4\ \delta_{\rm pr}^2 &= 3\left(\delta_{\rm pr}^2 + (\Gamma_{\rm a}/2)^2\right) \ , & (3.89) \\ \implies \delta_{\rm pr} &= \pm\frac{\sqrt{3}\Gamma_{\rm a}}{2} \ . & (3.90) \end{aligned}$$

On line centre, $\delta_{\rm pr} = 0$,

$$\frac{{\rm d}n_{\rm R}}{{\rm d}\omega_{\rm pr}} = -\frac{N{\rm d}_{\rm ba}^2}{2\epsilon_0\hbar} \cdot \frac{1}{(\Gamma_{\rm a}/2)^2} \ . \tag{3.91}$$

Whereas for $\delta_{\rm pr} = \pm\sqrt{3}\ (\Gamma_{\rm a}/2)$,

$$\frac{{\rm d}n_{\rm R}}{{\rm d}\omega_{\rm pr}} = \frac{N{\rm d}_{\rm ba}^2}{2\epsilon_0\hbar} \cdot \frac{1}{8\,(\Gamma_{\rm a}/2)^2} \ . \tag{3.92}$$

Hence $|{\rm d}n_{\rm R}/{\rm d}\omega|$ is at its greatest at line centre.

The line centre absorption can be derived from equations 2.88 and 2.94 on page 23.

$$\begin{aligned} \alpha(\delta_{\rm pr}=0) &= 2n_{\rm I}(\delta_{\rm pr}=0)k_{\rm ab} \ , \\ &= 2k_{\rm ab}\frac{N{\rm d}_{\rm ba}^2}{2\epsilon_0\hbar}\left(\frac{\Gamma_{\rm a}}{2}\right)^{-1} \ , \\ \Longrightarrow \quad \frac{\alpha(\delta_{\rm pr}=0)}{k_{\rm ab}\Gamma_{\rm a}} &= \frac{N{\rm d}_{\rm ba}^2}{2\epsilon_0\hbar} \cdot \frac{1}{(\Gamma_{\rm a}/2)^2} \ . \end{aligned} \tag{3.93}$$

Substituting equation 3.93 into 3.92 leads to,

$$\left.\frac{{\rm d}n_{\rm R}}{{\rm d}\omega_{\rm pr}}\right|_{\delta_{\rm pr}=0} = -\alpha(\delta_{\rm pr}=0)\frac{1}{k_{\rm ab}\Gamma_{\rm a}} \ . \tag{3.94}$$

Hence the line centre rate of change of the real part of the refractive index is directly proportional to the line centre absorption.

3.7.3 EIT Group Velocity

In the regime where the line shape of an EIT or EIA resonance is closely approximated by a Lorentzian function, then the results of the previous subsection can be used to determine the modification of the group velocity due to EIT or EIA. If the normalised transmission intensity of the EIT/EIA resonance, $I_{\rm EIT}$, is given by,

$$I_{\rm EIT} = I_{\rm BACK}\ {\rm e}^{-\alpha_{\rm EIT}z} \ , \tag{3.95}$$

where $I_{\rm BACK}$ is the intensity transmitted in the absence of the EIT/EIA resonance, it follows that,

$$\alpha_{\rm EIT} = \frac{1}{z}\ln\left|\frac{I_{\rm BACK}}{I_{\rm EIT}}\right| \ . \tag{3.96}$$

$\alpha_{\rm EIT}$ is specifically the modification to the absorption coefficient due to the EIT/EIA resonance.

In order to determine the dispersion, and hence the group velocity, concomitant with an EIT/EIA resonance at the centre of the that resonance, equation 3.96 has to be substituted into equation 3.94 . This leads to,

$$\left.\frac{{\rm d}n_{\rm R}}{{\rm d}\omega_{\rm pr}}\right|_{\delta_{\rm pr}=0} = -\frac{1}{z}\ln\left|\frac{I_{\rm BACK}}{I_{\rm EIT}}\right| \cdot \frac{\rm c}{\omega_{\rm ab}} \cdot \frac{1}{\Gamma_{\rm EIT}} \ , \tag{3.97}$$

$$\Longrightarrow \ {\rm v_g} = \frac{\rm c}{n_{\rm R} + ({\rm c}/z)\ln\left|\frac{I_{\rm EIT}}{I_{\rm BACK}}\right|(1/\Gamma_{\rm EIT})} \ , \tag{3.98}$$

where $\Gamma_{\rm EIT}$ is the FWHM of the EIT/EIA resonance.

In the work presented in this thesis the majority of measurements have been carried out on the $F = 1 \ \rightarrow \ F'$ hyperfine transitions of the ^{87}Rb D_2 line. In an 8 cm long Rb vapour cell at room temperature, as has been used throughout this work, this transition will give normalised transmission at the centre of the Doppler-broadened resonance of 0.9. Fig. 3.9 shows a plot of the predicted group velocity for a range of Lorentzian FWHM, $\Gamma_{\rm EIT}/2\pi$, of 40 kHz to 250 kHz and for normalised EIT amplitudes, $I_{\rm EIT} - I_{\rm BACK}$, of 0.01 to 0.045.

As can be seen in Fig. 3.9 the group velocity for a probe pulse is 0.006 c for an EIT resonance with FWHM 250 kHz and amplitude 0.01 . The group velocity falls to 2×10^{-4} c for a resonance of amplitude 0.045 with a FWHM 40 kHz.

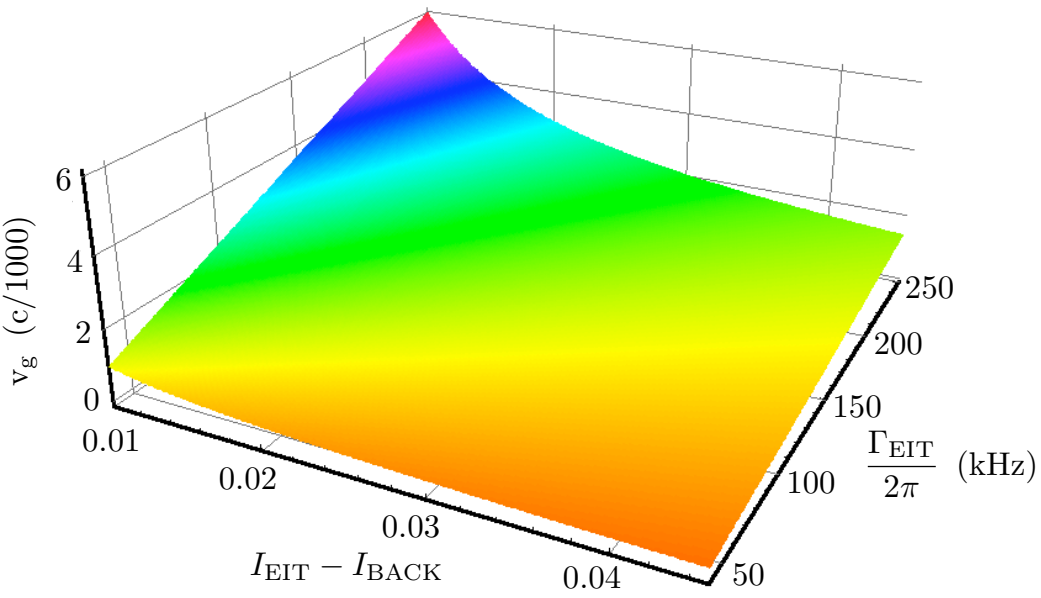

Figure 3.9: Theoretical plot of group velocity for ^{87}Rb vapour at room temperature in an 8 cm long vapour cell. The normalised transmission in the absence of the EIT feature is 0.9. The group velocity is shown for Lorentzian EIT features, with normalised amplitude ranging from 0.01 to 0.045 and FWHM form 40 kHz to 250 kHz.